THE JOURNAL OF BIOLOGICAL CHEMISTRY VOL. 287, NO. 22, pp. 18018–18029, May 25, 2012

Endoplasmic Reticulum Stress-associated Cone Photoreceptor Degeneration in Cyclic Nucleotide-gated Channel Deficiency*[S]

Received for publication, January 12, 2012, and in revised form, March 27, 2012 Published, JBC Papers in Press, April 9, 2012, DOI 10.1074/jbc.M112.342220

Arjun Thapa[‡], Lynsie Morris[‡], Jianhua Xu[‡1], Hongwei Ma[‡], Stylianos Michalakis[§], Martin Biel[§], and Xi-Qin Ding[‡2]

From the [‡]Department of Cell Biology, University of Oklahoma Health Sciences Center, Oklahoma City, Oklahoma 73104 and [§]Department of Pharmacy, The Center for Drug Research, Ludwig-Maximilians-Universität, Munich Center for Integrated Protein Science (CIPSM), 81377 München, Germany

Background: Photoreceptors undergo degeneration when phototransduction is impaired.
Results: The endoplasmic reticulum stress markers and processing of the associated caspases are elevated in retinas with cone photoreceptor CNG channel deficiency.
Conclusion: The endoplasmic reticulum stress-associated apoptotic pathways play a crucial role in cone degeneration.
Significance: Understanding of the mechanism(s) of photoreceptor degeneration is essential for development of therapeutic strategies.

Cyclic nucleotide-gated (CNG) channels play a pivotal role in phototransduction. Mutations in the cone CNG channel subunits CNGA3 and CNGB3 account for >70% of all known cases of achromatopsia. Cones degenerate in achromatopsia patients and in *CNGA3*$^{-/-}$ and *CNGB3*$^{-/-}$ mice. This work investigates the molecular basis of cone degeneration in CNG channel deficiency. As cones comprise only 2–3% of the total photoreceptor population in the wild-type mouse retina, we generated mouse lines with CNG channel deficiency on a cone-dominant background, *i.e.* *CNGA3*$^{-/-}$/*Nrl*$^{-/-}$ and *CNGB3*$^{-/-}$/*Nrl*$^{-/-}$ mice. The retinal phenotype and potential cell death pathways were examined by functional, biochemical, and immunohistochemical approaches. *CNGA3*$^{-/-}$/*Nrl*$^{-/-}$ and *CNGB3*$^{-/-}$/*Nrl*$^{-/-}$ mice showed impaired cone function, opsin mislocalization, and cone degeneration similar to that in the single knock-out mice. The endoplasmic reticulum stress marker proteins, including Grp78/Bip, phospho-eIF2α, phospho-IP$_3$R, and CCAAT/enhancer-binding protein homologous protein, were elevated significantly in *CNGA3*$^{-/-}$/*Nrl*$^{-/-}$ and *CNGB3*$^{-/-}$/*Nrl*$^{-/-}$ retinas, compared with the age-matched (postnatal 30 days) *Nrl*$^{-/-}$ controls. Along with these, up-regulation of the cysteine protease calpains and cleavage of caspase-12 and caspase-7 were found in the channel-deficient retinas, suggesting an endoplasmic reticulum stress-associated apoptosis. In addition, we observed a nuclear translocation of apoptosis-inducing factor (AIF) and endonuclease G in *CNGA3*$^{-/-}$/*Nrl*$^{-/-}$ and *CNGB3*$^{-/-}$/*Nrl*$^{-/-}$ retinas, implying a mitochondrial insult in the endoplasmic reticulum stress-activated cell death process. Taken together, our findings suggest a crucial role of endoplasmic reticulum stress in cone degeneration associated with CNG channel deficiency.

Rod and cone photoreceptor cyclic nucleotide-gated (CNG)[3] channels are localized to the plasma membrane of the outer segment (OS) and play a pivotal role in phototransduction. In darkness, rod CNG channels are activated by binding of cyclic guanosine monophosphate (cGMP), allowing a steady inward cation (Na^+ and Ca^{2+}) current. Light triggers a sequence of enzymatic reactions that leads to the hydrolysis of cGMP resulting in CNG channel closure, reduction of the inward cation (Na^+ and Ca^{2+}) currents, and membrane hyperpolarization (1). A similar transduction scheme exists in cones. Because it provides the only source of Ca^{2+} influx into the OS, the CNG channel is crucial to the control of intracellular Ca^{2+} concentration. Structurally, CNG channels belong to the superfamily of voltage-gated ion channels. The rod CNG channel is formed from CNGA1 and CNGB1 subunits, whereas the cone CNG channel is formed from CNGA3 and CNGB3 subunits. In the heterologous expression system, the A subunits by themselves form a functional channel, whereas the B subunits do not form channels in the absence of the A subunits. However, co-expression of the A and B subunits forms heteromeric channels displaying a number of properties of typical native CNG channels (1, 2). Biochemical characterization has demonstrated that the native photoreceptor CNG channels are the heterotetrameric complexes with a 3A:1B stoichiometry (3–6).

* This work was supported, in whole or in part, by NEI, National Institutes of Health Grants P30EY12190 and R01EY019490. This work was also supported by grants from the National Center for Research Resources (P20RR017703), the American Health Assistance Foundation, the Oklahoma Center for the Advancement of Science & Technology, and the Deutsche Forschungsgemeinschaft.
[S] This article contains supplemental Figs. 1 and 2.
[1] Present address: The Shanghai Institute of Planned Parenthood Research (SIPPR), 2140 Xie Tu Road, Xu Hui District, Shanghai, China.
[2] To whom correspondence should be addressed: Dept. of Cell Biology, University of Oklahoma Health Sciences Center, 940 Stanton L. Young Blvd., BMSB 553, Oklahoma City, OK 73104. Tel.: 405-271-8001 (ext. 47966); Fax: 405-271-3548; E-mail: xi-qin-ding@ouhsc.edu.

[3] The abbreviations used are: CNG, cyclic nucleotide-gated; AIF, apoptosis inducing factor; CHOP, CCAAT/-enhancer-binding protein homologous protein; Endo G, endonuclease G; ER, endoplasmic reticulum; IP$_3$R, inositol 1,4,5-trisphosphate receptor; phospho-IP$_3$R, phosphorylated form of IP$_3$R; ONL, outer nuclear layer; OS, outer segment; P30, postnatal day 30; PDE, phosphodiesterase; UPR, unfolded protein response.

Naturally occurring mutations in genes encoding CNGA3 and CNGB3 are highly associated with human cone diseases, including achromatopsia, progressive cone dystrophy, and early-onset macular degeneration (7–9). Indeed, >70 disease-associated mutations have been identified in *CNGA3* and *CNGB3* (8, 9), and these mutations account for >70% of achromatopsia patients (7, 8). Achromatopsia is a devastating hereditary visual disorder, characterized by deficient cone-mediated electroretinographic (ERG) responses, color blindness, visual acuity loss, pendular nystagmus, extreme light sensitivity, and daytime blindness. As the disease is primarily caused by mutations in CNG channel subunits, achromatopsia is often referred to as "channelopathy". Cone loss and degeneration in achromatopsia and cone dystrophy patients with CNG channel deficiency has been documented by optical coherence tomography studies (10–12). Impaired cone function and progressive cone degeneration has also been characterized in *CNGA3*$^{-/-}$ and *CNGB3*$^{-/-}$ mice (13–16). We have shown that photoreceptors undergo apoptotic death in CNG channel-deficient retinas (13, 16), similar to other types of inherited photoreceptor degeneration (17).

Photoreceptor degeneration is represented by two categories: induced degeneration such as that caused by bright light exposure (18) or retinal detachment (19) and inherited degeneration resulting from a variety of genetic disorders. Inherited rod and cone degeneration causes incurable visual diseases such as retinitis pigmentosa and cone dystrophy. Despite a remarkable genetic heterogeneity of photoreceptor degeneration, apoptotic cell death is recognized as a common pathway in many types of human retinal degeneration (17, 20). Recently, endoplasmic reticulum (ER) stress-associated apoptosis has been implicated in a wide variety of neuronal degenerative diseases, including retinal degeneration (20). The ER is a large membrane-enclosed cellular organelle in which membrane and secretory proteins are synthesized and folded into stable conformations and in which free Ca^{2+} ions are stored. Accumulation of incorrectly folded proteins in the ER is known to cause unfolded protein response (UPR) and ER stress, which often triggers cytotoxicity and cell death. ER stress-associated photoreceptor death has been shown in animal models of retinitis pigmentosa, including those caused by mutations in rhodopsin (such as P23H mutation) (21, 22) and by deficiency of the rod phosphodiesterase (PDE6, *rd* mice) (20, 23). Nevertheless, our understanding of the mechanism(s) of cone degeneration is limited, and we know little about the molecules and pathways involved in cone death in CNG channel deficiency. As CNG channel is the main source of the Ca^{2+} inward currents in the OS, deficiency of this channel may interfere with the cellular calcium homeostasis and lead to ER stress and subsequent cell death.

We investigated a potential role of ER stress in cone degeneration in CNG channel deficiency. An obvious challenge to study the cone system is the low population of cones in a rod-dominant mammalian retina. Cones comprise only 2–3% of the total photoreceptor population in the wild-type mouse retina. To overcome this, we generated mouse lines with CNG channel deficiency on a cone-dominant background, *i.e.* *CNGA3*$^{-/-}$/*Nrl*$^{-/-}$ and *CNGB3*$^{-/-}$/*Nrl*$^{-/-}$ mice. The double knock-out mice showed a retinal phenotype similar to that in their respective single knock-out mice, *i.e.* impaired cone function and cone degeneration. Biochemical characterization of the *CNGA3*$^{-/-}$/*Nrl*$^{-/-}$ and *CNGB3*$^{-/-}$/*Nrl*$^{-/-}$ mice (at postnatal 30 days) showed significantly elevated ER stress marker proteins, including Grp78/Bip, phospho-eIF2α, IP_3R, and CCAAT/enhancer-binding protein homologous protein (CHOP) in the retina. The up-regulation of the cysteine protease calpains and processing of caspase-12 and caspase-7 in *CNGA3*$^{-/-}$/*Nrl*$^{-/-}$ and *CNGB3*$^{-/-}$/*Nrl*$^{-/-}$ retinas suggest an ER stress-associated cell death process. Hence, ER stress might play a crucial role in cone degeneration in CNG channel deficiency.

EXPERIMENTAL PROCEDURES

Mice, Antibodies, and Other Materials—The *CNGA3*$^{-/-}$ and *CNGB3*$^{-/-}$ mouse lines (on a C57BL/6 background) were generated as described previously (14, 16). The *Nrl*$^{-/-}$ mouse line (on a C57BL/6 background) was kindly provided by Dr. Anand Swaroop (National Eye Institute, Bethesda, MD). The *CNGA3*$^{-/-}$/*Nrl*$^{-/-}$ and *CNGB3*$^{-/-}$/*Nrl*$^{-/-}$ mouse lines were generated by cross-mating. Wild-type mice (C57BL/6J background) were purchased from Charles River Laboratories (Wilmington, MA). All animal maintenance and experiments were approved by the local Institutional Animal Care and Use Committee (Oklahoma City, OK) and conformed to the guidelines on the care and use of animals adopted by the Society for Neuroscience and the Association for Research in Vision and Ophthalmology (Rockville, MD).

Primary antibodies used in this study are listed in Table 1. Horseradish peroxidase (HRP)-conjugated anti-rabbit and anti-mouse were purchased from Kirkegaard & Perry Laboratories, Inc. (Gaithersburg, MD). Fluorescent goat anti-rabbit and goat anti-mouse conjugated to Alexa Fluor 488, 568, or 647 were purchased from Invitrogen. All other reagents were purchased from Sigma, Bio-Rad, and Invitrogen.

Recordings of Electroretinograms (ERG)—Full-field ERG recordings were carried out as described previously (16). Briefly, after overnight dark adaptation, animals were anesthetized by intraperitoneal injection of 85 mg/kg ketamine and 14 mg/kg xylazine. ERGs were recorded using an LKC Technologies system (Gaithersburg, MD). Potentials were recorded using a platinum wire contacting the corneal surface through a layer of 2.5% methylcellulose. For assessment of scotopic responses, a white light stimulus intensity of 1.89 log cd s m^{-2} was presented to dark-adapted, dilated mouse eyes in a Ganzfeld (GS-2000; Nicolet Instruments, Inc. Madison, WI). To evaluate photopic responses, mice were adapted to a 1.46 log cd s m^{-2} light for 5 min, and then a light intensity of 1.89 log cd s m^{-2} was given (24). Responses were differentially amplified, averaged, and stored using a Nicolet Compact-4® signal averaging system. The ERG testing was performed between 10:00 a.m. and 12:00 p.m.

Retinal Protein Sample Preparation, SDS-PAGE, and Western Blot Analysis—Retinal protein sample preparation, SDS-PAGE, and Western blotting were performed as described previously (25). Briefly, retinas were homogenized in homogenization buffer (20 mM HEPES-NaOH, pH 7.4, 1 mM EDTA, 200 mM sucrose, containing protease mixture (Sigma)). The homo-

TABLE 1
List of antibodies used in this study

Antibody	Provider	Catalog no.	Dilutions used in immunoblotting
M-opsin	Dr. Cheryl Craft (Keck School of Medicine)		1:2000
Cone arrestin (CAR)	Dr. Cheryl Craft (Keck School of Medicine)		1:2000
S-opsin	Dr. Muna Naash (University of Oklahoma Health Sciences Center)		1:1000
CNGA3	Custom antibody generated by YenZym Antibodies, LLC (Ref. 25)		1:250
Gnat2	Santa Cruz Biotechnology	sc-390	1:500
GADD 153 (CHOP-10)	Santa Cruz Biotechnology	sc-575	1:100
Phospho-eIF2α	Cell Signaling Technology	3398	1:500
Phospho-IP_3 R	Cell Signaling Technology	3760	1:250
Caspase-7	Cell Signaling Technology	9492	1:250
Caspase-12	Cell Signaling Technology	2202	1:250
Endo G	Cell Signaling Technology	4969	1:250
AIF	Cell Signaling Technology	4642	1:500
Cytochrome *c*	Cell Signaling Technology	4272	1:250
Caspase-9	Cell Signaling Technology	9504	1:250
Caspase-3	Cell Signaling Technology	9661	1:250
Calpain II	Cell Signaling Technology	2539	1:500
Bcl-2	Epitomic	1017-1	1:250
Bcl-2-x_L	Epitomic	1018-1	1:250
Calpain I	Abcam	ab28258	1:500
Grp78/BiP	Abcam	ab21685	1:500
β-Actin	Abcam	ab-6276	1:2000
Acetyl-histone H3 (H3)	Upstate Cell Signaling Solution	07-540	1:2000
TATA binding protein	Thermo Scientific, Inc.	MA1-10883	1:500

genate was centrifuged at 1000 × *g* for 10 min at 4 °C to pellet down nuclei and cell debris. The pellet was used as nuclei-enriched fraction after three washes. The supernatant of the homogenate was further centrifuged at 16,000 × *g* for 30 min at 4 °C to separate out cytosolic (supernatant) and membrane fractions (pellet). Protein concentration of the preparations was measured using a Bio-Rad Protein Assay kit (Bio-Rad Laboratories).

The protein samples (8 to 20 μg) were solubilized in SDS-PAGE sample buffer and separated on an SDS-PAGE gel (7 or 10% acrylamide) and transferred onto polyvinylidene difluoride (PVDF) membrane (Bio-Rad Laboratories). After 1 h of blocking in 5% milk or 5% BSA containing Tris-buffered saline with 0.1% Tween (v/v) at room temperature, the membranes were incubated with primary antibodies overnight at 4 °C (see Table 1 for antibody dilutions). The membranes were then washed with Tris-buffered saline with 0.1% Tween three to four times and incubated with HRP-conjugated secondary anti-rabbit or anti-mouse antibodies for 1 h at room temperature. After washing, the antigen and antibody binding was detected using SuperSignal® West Dura Extended Duration chemiluminescent substrate (Pierce). The blots were scanned, and images were captured using a KODAK Image Station 4000R digital imaging system (Carestream Molecular Imaging, New Haven, CT). Densitometry analysis was performed by quantifying the intensities of the bands of interest using KODAK molecular imaging software with β-actin or acetyl-histone H3 serving as a loading control. Data for each group were obtained from three to four independent Western blot experiments performed using retinas prepared from four to five mice and analyzed and graphed using GraphPad Prism® software (GraphPad Software, San Diego, CA).

Eye Preparation, Immunofluorescence Labeling, and Confocal Microscopy—Mouse eye cross-sections were prepared for immunohistochemical analysis as described previously (16). Briefly, euthanasia of mice was performed by CO_2 asphyxiation, and mouse eyes were enucleated and fixed with 4% formaldehyde (Polysciences, Inc., Warrington, PA) in 0.1 M sodium phosphate buffer, pH 7.4, for 16 h at 4 °C. The superior portion of the cornea was marked with a green dye for orientation prior to enucleation. Fixed eyes were transferred to PBS or 0.1 M sodium phosphate buffer, pH 7.4, containing 0.02% sodium azide, for storage until processing and embedding in paraffin. Paraffin sections (5-μm thickness) passing vertically through the retina were prepared using a Leica microtome (Richmond, IL). Immunofluorescence labeling was performed as described previously (16). Briefly, eye sections were blocked with PBS containing 5% BSA and 0.5% Triton X-100 for 1 h at room temperature. When necessary, antigen retrieval was performed by incubating tissues in 10 mM sodium citrate buffer, pH 6.0, for 30 min in a 65 °C water bath. Primary antibody incubation (rabbit anti-CHOP, 1:200; goat anti-S-opsin, 1:500; and rabbit anti-Grp78/Bip, 1:200) was performed at room temperature for 2 h. Following Alexa Fluor 488 or 568 or FITC-conjugated secondary antibody incubation and rinses, slides were mounted and coverslipped. Fluorescent signals were imaged using an Olympus AX70 fluorescence microscope (Olympus Corp., Center Valley, PA) with QCapture imaging software (QImaging Corp., Surrey, BC, Canada) or an Olympus IX81-FV500 confocal laser scanning microscope (Olympus, Melville, NY) (using excitation wavelengths of 543 nm for Alexa Fluor 568 and 488 nm for FITC) and FluoView imaging software (Olympus, Melville, NY).

TUNEL Assay—The TUNEL assay was performed to evaluate photoreceptor apoptotic death in *CNGA3*$^{-/-}$/*Nrl*$^{-/-}$, *CNGB3*$^{-/-}$/*Nrl*$^{-/-}$ and *Nrl*$^{-/-}$ mice as described previously (16). An apoptosis detection kit (ApopTag plus peroxidase *in situ* apoptosis detection; Chemicon, Temecula, CA) and paraffin-embedded sections were used in this analysis. Immunohistochemical labeling was imaged using an Olympus AX70 fluorescence microscope (Olympus Corp.) with QCapture imaging software (QImaging Corp.). Quantification of the positive labeling was performed by using Image Pro 6® software (Media Cybernetics, Inc., Bethesda, MD). Briefly, images were taken

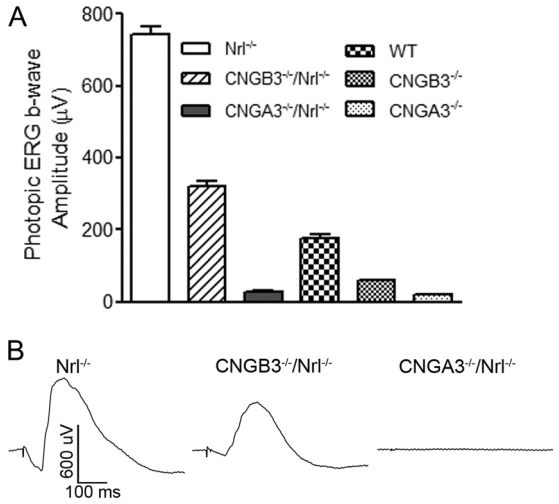

FIGURE 1. **Impaired cone function in *CNGA3*$^{-/-}$/*Nrl*$^{-/-}$ and *CNGB3*$^{-/-}$/*Nrl*$^{-/-}$ mice.** ERG was performed to evaluate the retinal function in mice at P30. Shown are amplitudes of the photopic ERG b-wave responses in *Nrl*$^{-/-}$, *CNGB3*$^{-/-}$/*Nrl*$^{-/-}$, *CNGA3*$^{-/-}$/*Nrl*$^{-/-}$, wild-type, *CNGB3*$^{-/-}$, and *CNGA3*$^{-/-}$ mice (*A*) and representative photopic ERG traces in *Nrl*$^{-/-}$, *CNGB3*$^{-/-}$/*Nrl*$^{-/-}$, and *CNGA3*$^{-/-}$/*Nrl*$^{-/-}$ mice (*B*). Data are represented as means ± S.E. of four independent measurements from six to ten mice.

using a 40× objective on an Olympus microscope; the image scale was calibrated; and positive labeling was counted in regions with dimensions of 336 × 256 μm (8.6 × 10^4 μm^2) using the software. The averages from four to five regions of each retinal section were obtained, and data from sections were prepared from four to five mice from each group were analyzed and graphed using GraphPad Prism® software (GraphPad Software).

RESULTS

Impaired Cone Function in CNGA3$^{-/-}$/*Nrl*$^{-/-}$ *and CNGB3*$^{-/-}$/*Nrl*$^{-/-}$ *Mice*—We have previously shown an impaired cone function and cone degeneration in *CNGA3*$^{-/-}$ (13, 14) and *CNGB3*$^{-/-}$ mice (15, 16). To study the mechanism of cone degeneration, we generated the double knock-out *CNGA3*$^{-/-}$/*Nrl*$^{-/-}$ and *CNGB3*$^{-/-}$/*Nrl*$^{-/-}$ mouse lines, which have CNG channel deficiency on a cone-dominant background. We first examined the retinal phenotype of these mice. Retinal function was evaluated by ERG recordings. Fig. 1*A* shows the amplitudes of photopic ERG b-wave responses in *CNGA3*$^{-/-}$/*Nrl*$^{-/-}$, *CNGB3*$^{-/-}$/*Nrl*$^{-/-}$ and *Nrl*$^{-/-}$ mice at postnatal 30 days (P30). The ERG responses for *CNGA3*$^{-/-}$, *CNGB3*$^{-/-}$, and wild-type are shown for comparison. Fig. 1*B* shows representative photopic ERG traces in *Nrl*$^{-/-}$, *CNGB3*$^{-/-}$/*Nrl*$^{-/-}$, and *CNGA3*$^{-/-}$/*Nrl*$^{-/-}$ mice. Similar to their respective single knock-out mice, *CNGA3*$^{-/-}$/*Nrl*$^{-/-}$ mice showed lack of cone function, whereas the ERG response was reduced by ~60% in *CNGB3*$^{-/-}$/*Nrl*$^{-/-}$ mice, compared with the age-matched *Nrl*$^{-/-}$ mice. As expected, no significant scotopic light response was detected in *Nrl*$^{-/-}$, *CNGA3*$^{-/-}$/*Nrl*$^{-/-}$, or *CNGB3*$^{-/-}$/*Nrl*$^{-/-}$ mice, due to *Nrl* deficiency (data not shown).

Reduced Expression of Cone Opsin and Other Phototransduction Proteins in CNGA3$^{-/-}$/*Nrl*$^{-/-}$ *and CNGB3*$^{-/-}$/*Nrl*$^{-/-}$ *Mice*—*CNGA3*$^{-/-}$ and *CNGB3*$^{-/-}$ mice develop cone degeneration, manifested as reduced levels of cone specific proteins and decreased cone density (13, 15). We examined retinal expression levels of M-opsin, S-opsin, cone arrestin, and cone transducing subunit α-2 (Gnat2) in *CNGA3*$^{-/-}$/*Nrl*$^{-/-}$, *CNGB3*$^{-/-}$/*Nrl*$^{-/-}$, and *Nrl*$^{-/-}$ mice at P30. Western blot analysis showed significantly reduced levels of these proteins in *CNGA3*$^{-/-}$/*Nrl*$^{-/-}$ and *CNGB3*$^{-/-}$/*Nrl*$^{-/-}$ retinas (Fig. 2*A*). The expression levels of M-opsin, S-opsin, Gnat2, and cone arrestin were reduced by ~45, 34, 26, and 46%, respectively, in *CNGA3*$^{-/-}$/*Nrl*$^{-/-}$ mice, and reduced by ~28, 24, 28, and 33%, respectively, in *CNGB3*$^{-/-}$/*Nrl*$^{-/-}$ mice, compared with the age-matched *Nrl*$^{-/-}$ controls (Fig. 2, *B–E*). Hence, *CNGA3*$^{-/-}$/*Nrl*$^{-/-}$ and *CNGB3*$^{-/-}$/*Nrl*$^{-/-}$ mice resemble their respective single knock-out mice, showing impaired cone function and cone degeneration.

Photoreceptor Death in CNGA3$^{-/-}$/*Nrl*$^{-/-}$ *and CNGB3*$^{-/-}$/*Nrl*$^{-/-}$ *Mice*—Previous studies have shown the enhanced TUNEL-positive labeling in *CNGA3*$^{-/-}$ and *CNGB3*$^{-/-}$ mice (13, 16). We performed TUNEL assay on the retinal sections of *CNGA3*$^{-/-}$/*Nrl*$^{-/-}$ and *CNGB3*$^{-/-}$/*Nrl*$^{-/-}$ mice at the ages of P10, P15, P30, and P60. As expected, we observed a significantly enhanced TUNEL-positive labeling in *CNGA3*$^{-/-}$/*Nrl*$^{-/-}$ and *CNGB3*$^{-/-}$/*Nrl*$^{-/-}$ retinas. At P10, the TUNEL-positive labeling in the double knock-out mice showed no difference from the *Nrl*$^{-/-}$ mice, suggesting a development-related photoreceptor death at this age. However, significantly more TUNEL-positive labeling was observed in *CNGA3*$^{-/-}$/*Nrl*$^{-/-}$ and *CNGB3*$^{-/-}$/*Nrl*$^{-/-}$ retinas at P15 and P30 days (Fig. 3*A*). Quantitative analysis showed that the TUNEL-positive cells in CNG channel-deficient mice at P15 were increased 2–3-fold, compared with the age-matched *Nrl*$^{-/-}$ controls (Fig. 3*B*). No TUNEL-positive labeling was detected in *CNGA3*$^{-/-}$/*Nrl*$^{-/-}$, *CNGB3*$^{-/-}$/*Nrl*$^{-/-}$, and *Nrl*$^{-/-}$ retinas at P60 (data not shown). Hence, similar to the single knock-out mice, photoreceptors in *CNGA3*$^{-/-}$/*Nrl*$^{-/-}$ and *CNGB3*$^{-/-}$/*Nrl*$^{-/-}$ mice undergo apoptotic death as early as P15 days. It is worth mentioning that the TUNEL-positive labeling in *Nrl*$^{-/-}$ retina is similar to that in the age-matched wild-type mice (26).

Enhanced Expression of ER Stress Marker Proteins in CNGA3$^{-/-}$/*Nrl*$^{-/-}$ *and CNGB3*$^{-/-}$/*Nrl*$^{-/-}$ *Retinas*—As CNG channel plays a key role in OS calcium homeostasis; loss of the functional channel is likely to alter the cellular calcium balance. Moreover, cones in CNG channel-deficient mice display opsin mislocalization, accompanied by photoreceptor apoptotic death. Hence, we examined whether there is ER stress in CNG channel-deficient retinas. The expression levels of the ER stress marker proteins, Grp78/Bip, phospho-eIF2α, and CHOP were examined by immunoblotting. Grp78/Bip is a member of the heat-shock protein-70 family and is involved in the folding and assembly of proteins in the ER. Grp78/Bip interacts transiently with many ER proteins and plays a key role in monitoring protein transport through the cell. When there is ER overload and stress, Grp78/Bip dissociates from its interacting proteins (such as protein kinase RNA-like endoplasmic reticulum kinase), initiating activation or phosphorylation of a variety of proteins, including eIF2 (eukaryotic initiation factor 2, a protein required in the initiation of translation) (27). Here, we show the elevated levels of the ER stress markers in *CNGA3*$^{-/-}$/*Nrl*$^{-/-}$ and *CNGB3*$^{-/-}$/*Nrl*$^{-/-}$ retinas. As shown in Fig. 4*A*, the levels

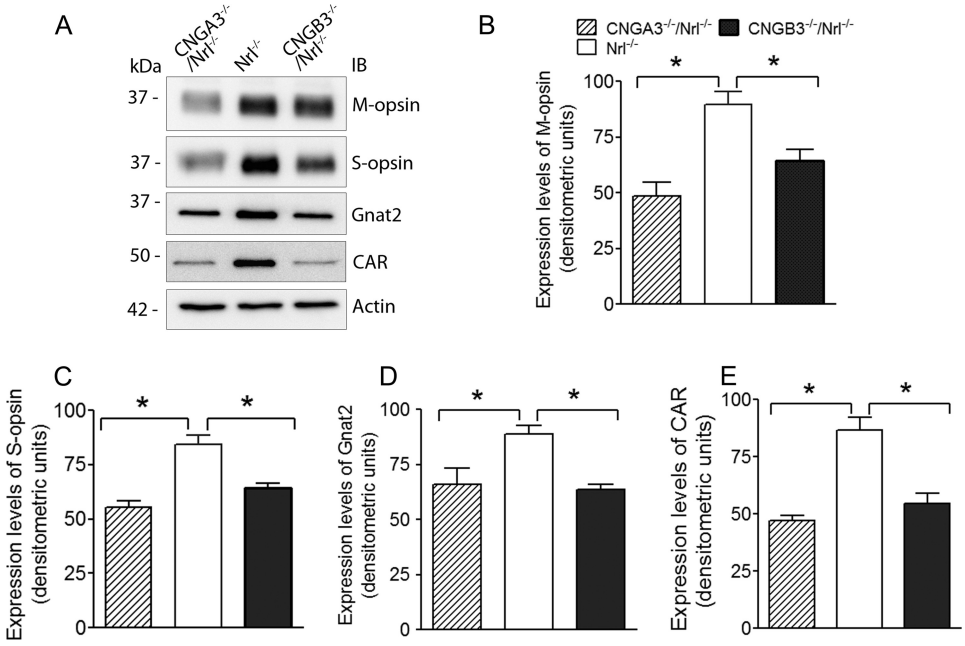

FIGURE 2. **Reduced expression of cone opsin and other phototransduction proteins in *CNGA3*$^{-/-}$/*Nrl*$^{-/-}$ *and CNGB3*$^{-/-}$/*Nrl*$^{-/-}$ mice.** Western blot was performed to detect retinal expression of M-opsin, S-opsin, cone arrestin (*CAR*), and Gnat2 in *CNGA3*$^{-/-}$/*Nrl*$^{-/-}$, *CNGB3*$^{-/-}$/*Nrl*$^{-/-}$, and *Nrl*$^{-/-}$ mice at P30. Shown are representative images (*A*) and the correlating densitometric analysis (*B–E*). Actin was probed as a loading control. Data are represented as means ± S.E. of measurements from three to four independent experiments using retinas from four to five mice. Unpaired Student's *t* test was used for determination of the significance (*, $p < 0.05$).

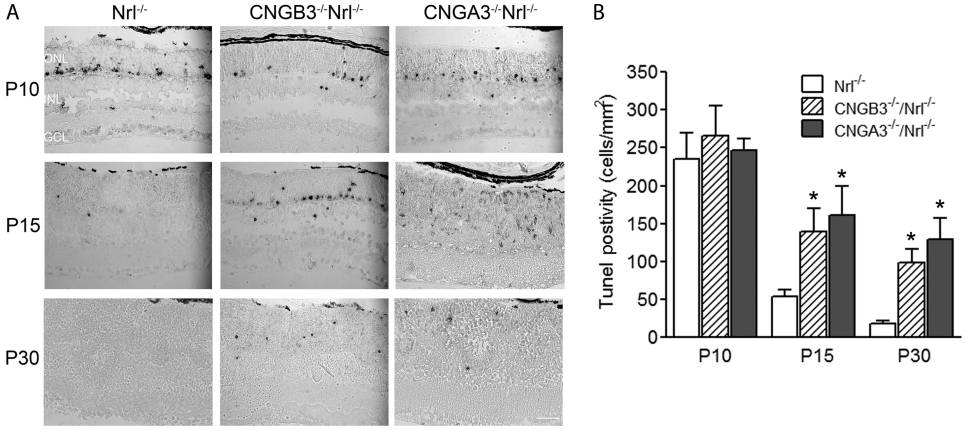

FIGURE 3. **Photoreceptor death in *CNGA3*$^{-/-}$/*Nrl*$^{-/-}$ and *CNGB3*$^{-/-}$/*Nrl*$^{-/-}$ mice.** TUNEL assay was performed using retinal sections prepared from *CNGA3*$^{-/-}$/*Nrl*$^{-/-}$, *CNGB3*$^{-/-}$/*Nrl*$^{-/-}$, and *Nrl*$^{-/-}$ mice at P10, P15, and P30. *A*, representative images showing TUNEL-positive cells. *ONL*, outer nuclear layer; *INL*, inner nuclear layer; *GCL*, ganglion cell layer. *Scale bar*, 50 μm. *B*, quantitative analysis of nuclear fragmentation in the ONL of *CNGA3*$^{-/-}$/*Nrl*$^{-/-}$, *CNGB3*$^{-/-}$/*Nrl*$^{-/-}$, and *Nrl*$^{-/-}$ retinas. The means ± S.E. were obtained from three to four mice in each group (two to three sections from each mouse).

of Grp78/Bip and phospho-eIF2α were increased significantly in *CNGA3*$^{-/-}$/*Nrl*$^{-/-}$ and *CNGB3*$^{-/-}$/*Nrl*$^{-/-}$ retinas. Densitometric analysis shows that the levels of phospho-eIF2α were enhanced by ~38 and 20% in *CNGA3*$^{-/-}$/*Nrl*$^{-/-}$ and *CNGB3*$^{-/-}$/*Nrl*$^{-/-}$ retinas, respectively, compared with the *Nrl*$^{-/-}$ control (Fig. 4*A*). CHOP (also known as GADD153 (growth arrest and DNA damage-inducible protein 153)) is a member of the C/EBP (CCAAT enhancer-binding protein) transcription factor family and functions as a dimer to inhibit the DNA-binding activity of C/EBP and liver-enriched activator protein. This protein is not expressed at detectable levels under normal conditions and is induced in ER stress through the Grp78/Bip-phospho-eIF2α pathway (28). We therefore examined CHOP expression using retinal nuclear preparations and found that the expression levels of CHOP were increased in *CNGA3*$^{-/-}$/*Nrl*$^{-/-}$ and *CNGB3*$^{-/-}$/*Nrl*$^{-/-}$ retinas (Fig. 4*A*). The elevated CHOP expression was also shown by immunofluorescence labeling. The CHOP signal was barely detected in the ONL of *Nrl*$^{-/-}$ retinas (Fig. 4*B*, *left panel*); in contrast, a markedly increased signal was detected in the ONL of *CNGA3*$^{-/-}$/*Nrl*$^{-/-}$ retinas (Fig. 4*B*, *right panel*).

We have shown opsin mislocalization in CNG channel-deficient retina (13, 15). To determine whether opsin is mislocalized in the ER, we performed double labeling on retinal sections of *CNGA3*$^{-/-}$, *CNGB3*$^{-/-}$, and wild-type mice using anti-Grp78/Bip and anti-S-opsin. Analysis of high magnification images of confocal microscopy shows a co-labeling of S-opsin and Grp78/Bip in the inner segment of *CNGA3*$^{-/-}$ and *CNGB3*$^{-/-}$ but not wild-type retina, and both proteins are barely detected in the inner segment of the wild-type mice (Fig. 4*C*).

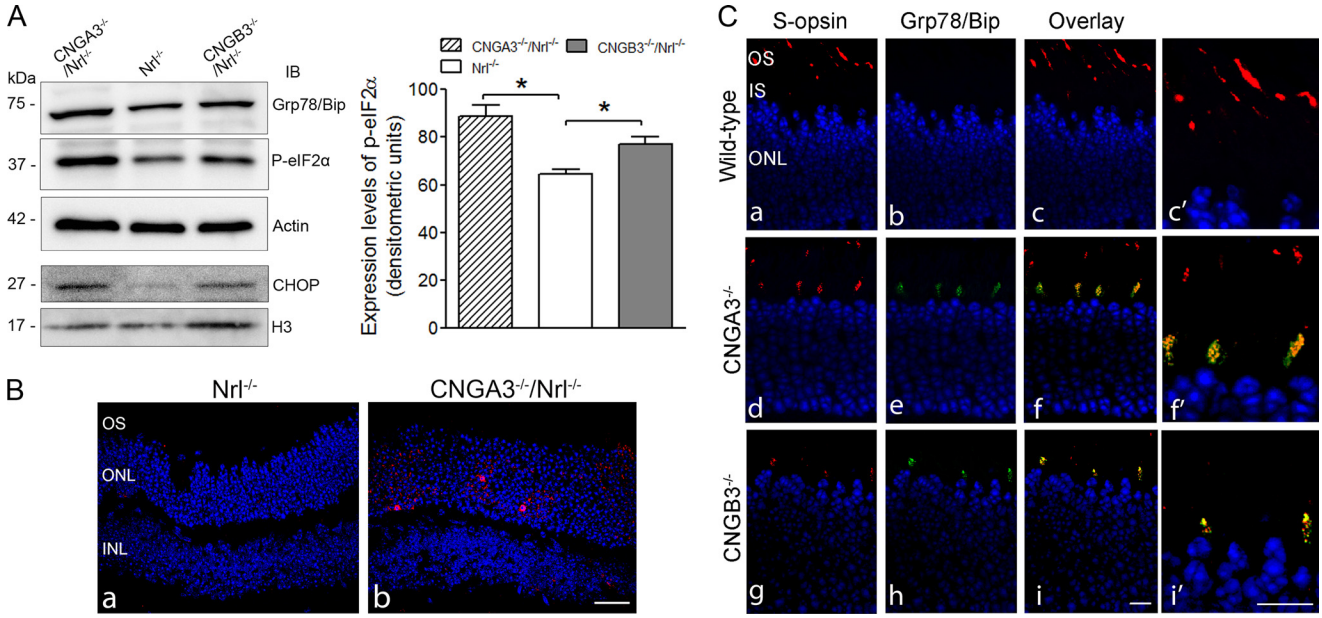

FIGURE 4. **Enhanced expression of the ER stress marker proteins in *CNGA3*$^{-/-}$/*Nrl*$^{-/-}$ and *CNGB3*$^{-/-}$/*Nrl*$^{-/-}$ retinas.** The expression levels of Grp78/Bip, phospho-eIF2α, and CHOP were examined in *CNGA3*$^{-/-}$/*Nrl*$^{-/-}$, *CNGB3*$^{-/-}$/*Nrl*$^{-/-}$, and *Nrl*$^{-/-}$ mice at P30. *A*, *left panel*: shown are representative images of the Western blot detections. Total retinal protein lysate was used for detection of Grp78/Bip and phospho-eIF2α (actin was used as a loading control, *upper three panels*), and retinal nuclear preparation was used for detection of CHOP. (H3 was used as a loading control, *lower two panels*.) *Right panel*: densitometric analysis of the relative expression levels of phospho-eIF2α in *CNGA3*$^{-/-}$/*Nrl*$^{-/-}$, *CNGB3*$^{-/-}$/*Nrl*$^{-/-}$, and *Nrl*$^{-/-}$ retinas. Data are represented as means ± S.E. of measurements from three to four independent experiments using retinas from four to five mice. Unpaired Student's *t* test was used for determination of the significance (*, $p < 0.05$). *B*, CHOP activation in CNG channel-deficient retina. Shown are images of CHOP staining on retinal sections of *Nrl*$^{-/-}$ (*a*) and *CNGA3*$^{-/-}$/*Nrl*$^{-/-}$ (*b*) mice. *C*, co-localization of Grp78/Bip with S-opsin in CNG channel-deficient retina. Co-labeling was performed using rabbit anti-Grp78/Bip and goat anti-S-opsin antibodies. Shown are images of the co-labeling on retinal sections of WT (*a–c*), *CNGA3*$^{-/-}$ (*d–f*), and *CNGB3*$^{-/-}$ (*g–i*) mice with higher magnification images alongside (*c′*, *f′*, *i′*). *IS*, inner segment; *ONL*, outer nuclear layer; *IB*, immunoblot. *Scale bar*, 20 μm.

Enhanced Levels of Phospho-IP$_3$R and Calpains in CNGA3$^{-/-}$/*Nrl*$^{-/-}$ *and CNGB3*$^{-/-}$/*Nrl*$^{-/-}$ *Retinas*—Inositol 1,4,5-trisphosphate (IP$_3$) is a second messenger for many growth factors, hormones, and neurotransmitters. Upon binding to its receptor (IP$_3$R) on the ER membrane, IP$_3$ triggers the phosphorylation of IP$_3$R. In the channel-deficient photoreceptors there is an altered calcium balance, which may stimulate the release of Ca^{2+} from the ER store. Therefore, we examined the levels of phospho-IP$_3$R, and we found its elevation in *CNGA3*$^{-/-}$/*Nrl*$^{-/-}$ and *CNGB3*$^{-/-}$/*Nrl*$^{-/-}$ retinas (Fig. 5*A*). Densitometric analysis showed that the levels of phospho-IP$_3$R were enhanced ~30 and 27% in *CNGA3*$^{-/-}$/*Nrl*$^{-/-}$ and *CNGB3*$^{-/-}$/*Nrl*$^{-/-}$ mice, respectively, compared with the *Nrl*$^{-/-}$ controls (Fig. 5*B*). We further examined the expression levels of the cysteine protease calpains (calpain I and calpain II, also known as μ-calpain and *m*-calpain) in the channel-deficient retinas. Calpains have been shown to be activated by Ca^{2+} under ER stress and are involved in the processing of caspase-12 (29). As shown in Fig. 5*A*, expression levels of these proteases were increased significantly in *CNGA3*$^{-/-}$/*Nrl*$^{-/-}$ and *CNGB3*$^{-/-}$/*Nrl*$^{-/-}$ retinas. Densitometric analysis showed that the levels of calpain II were enhanced by ~28 and 19% in *CNGA3*$^{-/-}$/*Nrl*$^{-/-}$ and *CNGB3*$^{-/-}$/*Nrl*$^{-/-}$ retinas, respectively (Fig. 5*B*). It has also been shown that the ER membrane permeability to Ca^{2+} is altered by activation of the Bcl-2 proteins in cells undergoing apoptotic death (30). We therefore examined the expression levels of Bcl-2 and Bcl-x and found a significant elevation of these proteins in *CNGA3*$^{-/-}$/*Nrl*$^{-/-}$ retina (Fig. 5*C*). This result along with an elevated phospho-IP$_3$R supports a potential Ca^{2+} release from ER storage in CNG channel-deficient cones.

Enhanced Processing of Caspase-12 in CNGA3$^{-/-}$/*Nrl*$^{-/-}$ *and CNGB3*$^{-/-}$/*Nrl*$^{-/-}$ *Retinas*—We found evidence of ER stress in *CNGA3*$^{-/-}$/*Nrl*$^{-/-}$ and *CNGB3*$^{-/-}$/*Nrl*$^{-/-}$ retinas and further examined whether this ER stress is associated with cone death. It has been shown that the cysteine protease caspase-12 is activated upon ER stress and Ca^{2+} release from the ER store, and its processed forms can translocate into the nucleus to induce apoptosis (31, 32). Therefore, we examined the levels of caspase-12 and its processing in the CNG channel-deficient retina. The processing of the protein was evaluated by Western blotting using an antibody recognizing the full-length protein and its cleaved products. As shown in Fig. 6*A*, procaspase-12 was detected in the retinal cytosols only, whereas the cleaved forms were detected in both cytosolic and nuclear fractions. The expression levels of procaspase-12 in *CNGA3*$^{-/-}$/*Nrl*$^{-/-}$ and *CNGB3*$^{-/-}$/*Nrl*$^{-/-}$ retina were similar to that in *Nrl*$^{-/-}$ retina; however, significantly elevated levels of the cleaved forms were detected in *CNGA3*$^{-/-}$/*Nrl*$^{-/-}$ and *CNGB3*$^{-/-}$/*Nrl*$^{-/-}$ retinas, which was particularly obvious in the nuclei-enriched preparations (Fig. 6*A*). Densitometric analysis showed that the levels of the cleaved forms were enhanced by ~33 and 15% in *CNGA3*$^{-/-}$/*Nrl*$^{-/-}$ and *CNGB3*$^{-/-}$/*Nrl*$^{-/-}$ mice, respectively (Fig. 6*B*). Thus, CNG channel-deficient retinas show an enhanced processing of caspase-12, suggesting an ER stress-associated, caspase-12-mediated cell death process.

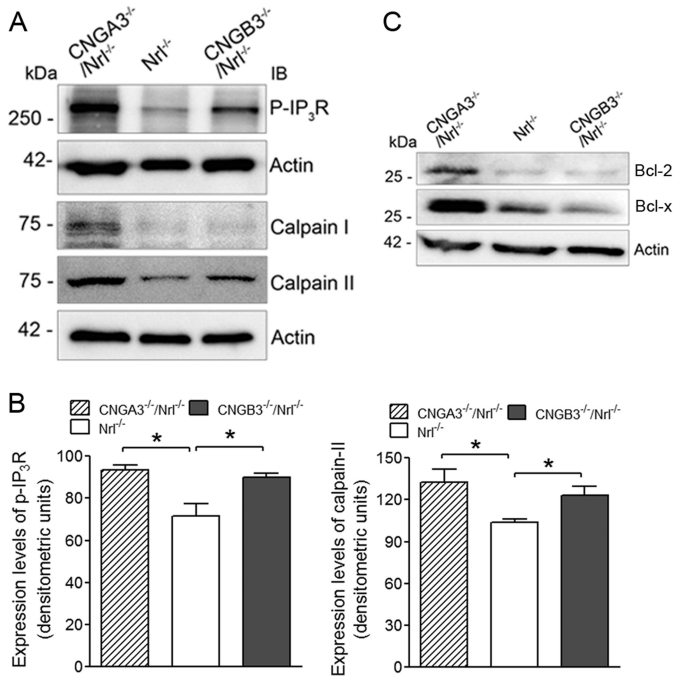

FIGURE 5. **Enhanced levels of phospho-IP$_3$R and calpains in *CNGA3*$^{-/-}$/*Nrl*$^{-/-}$ and *CNGB3*$^{-/-}$/*Nrl*$^{-/-}$ retinas.** The expression levels of phospho-IP$_3$R, calpain I, and calpain II were examined in *CNGA3*$^{-/-}$/*Nrl*$^{-/-}$, *CNGB3*$^{-/-}$/*Nrl*$^{-/-}$, and *Nrl*$^{-/-}$ mice at P30. *A*, shown are representative images of the Western blot detections. Total retinal protein lysate was used for the detections, and actin was used as loading control. *B*, densitometric analysis of the relative expression levels of phospho-IP$_3$R (*left panel*) and calpain II (*right panel*) in *CNGA3*$^{-/-}$/*Nrl*$^{-/-}$, *CNGB3*$^{-/-}$/*Nrl*$^{-/-}$, and *Nrl*$^{-/-}$ retinas. Data are represented as means ± S.E. of measurements from three to four independent experiments using retinas from four to five mice. Unpaired Student's *t* test was used for determination of the significance (*, $p < 0.05$). *C*, shown are representative images of the Western blot detections of Bcl-2 and Bcl-x in the mouse retina. Total retinal protein lysate was used, and actin was used as a loading control.

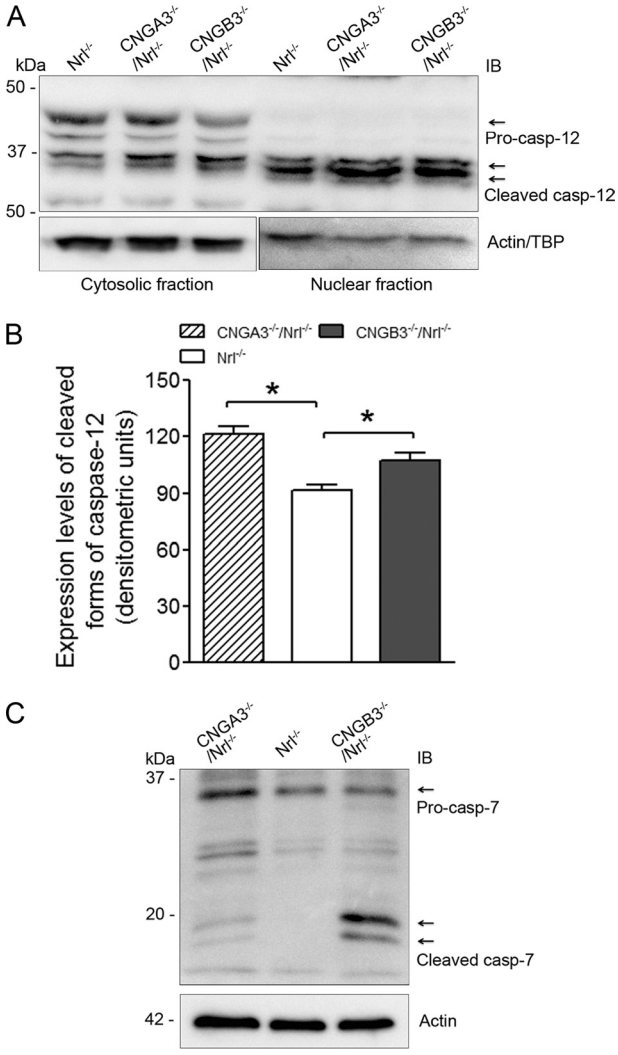

FIGURE 6. **Enhanced processing of caspase-12 and cleavage of caspase-7 in *CNGA3*$^{-/-}$/*Nrl*$^{-/-}$ and *CNGB3*$^{-/-}$/*Nrl*$^{-/-}$ retinas.** The expression levels of caspase-12 and caspase-7 and their processed forms were examined in *CNGA3*$^{-/-}$/*Nrl*$^{-/-}$, *CNGB3*$^{-/-}$/*Nrl*$^{-/-}$, and *Nrl*$^{-/-}$ mice at P30. *A*, shown are representative images of the Western blot detection of caspase-12. Both cytosolic and nuclear fractions were used for this examination. Actin and TATA binding protein were used as loading controls for cytosolic and nuclear fractions, respectively. *B*, densitometric analysis of the relative levels of processed forms of caspase-12 (*casp-12*) in the nuclear fractions of *CNGA3*$^{-/-}$/*Nrl*$^{-/-}$, *CNGB3*$^{-/-}$/*Nrl*$^{-/-}$, and *Nrl*$^{-/-}$ retina. Data are represented as means ± S.E. of measurements from three to four independent experiments using retinas from four to five mice. Unpaired Student's *t* test was used for determination of the significance (*, $p < 0.05$). *C*, shown are representative images of the Western blot detection of caspase-7. Retinal cytosolic protein preparations were used for this examination. Actin was used as a loading control. *IB*, immunoblot.

Furthermore, caspase-7, which resides in the ER neighborhood along with caspase-12, can also be activated under ER stress (33) and can subsequently cleave procaspase-12 to generate active forms of the protease (34). We therefore examined the levels of caspase-7 and its cleaved products. The full-length protein was detected in the retinal cytosolic preparations of both channel-deficient and control mice; however, the cleaved forms were detected only in *CNGA3*$^{-/-}$/*Nrl*$^{-/-}$ and *CNGB3*$^{-/-}$/*Nrl*$^{-/-}$ retinas (Fig. 6*C*), suggesting an activation of caspase-7. We did not detect any caspase-7 immunoreactivity in the nuclear fractions (data not shown), suggesting that caspase-7 may act only as an initiating (activating) protease.

Expression of Mitochondrial Apoptotic Proteins in CNGA3$^{-/-}$/*Nrl*$^{-/-}$ *and CNGB3*$^{-/-}$/*Nrl*$^{-/-}$ *Retinas*—Although we obtained evidence supporting the ER stress and ER stress-associated apoptotic death process in *CNGA3*$^{-/-}$/*Nrl*$^{-/-}$ and *CNGB3*$^{-/-}$/*Nrl*$^{-/-}$ retina, it was tempting to test whether mitochondrial-associated cell death is involved. Apoptosis-inducing factor (AIF) is the protein that triggers chromatin condensation and DNA degradation. Normally, it is found behind the outer membrane of the mitochondria and therefore is sheltered from the nucleus. When the mitochondria are damaged, it moves to the cytosol and to the nucleus and initiates a caspase-independent cell death process. We therefore examined the expression levels of AIF in the retinal nuclear and cytosolic fractions. We found a significant elevation of AIF in the nuclear fractions of *CNGA3*$^{-/-}$/*Nrl*$^{-/-}$ and *CNGB3*$^{-/-}$/*Nrl*$^{-/-}$ retinas, compared with the *Nrl*$^{-/-}$ controls (Fig. 7*A*), and only a trace amount of the protein was detected in the cytosol fractions of both channel-deficient and *Nrl*$^{-/-}$ retinas (data not shown). We also examined the nuclear translocation of endonuclease G (Endo G), an endonuclease that is localized in the mitochondrion and has been shown to act as an apoptotic DNase when released from mitochondria (35). As shown in Fig. 7*A*, expression levels of Endo G in the nuclear fractions of the channel-deficient retina were increased significantly, com-

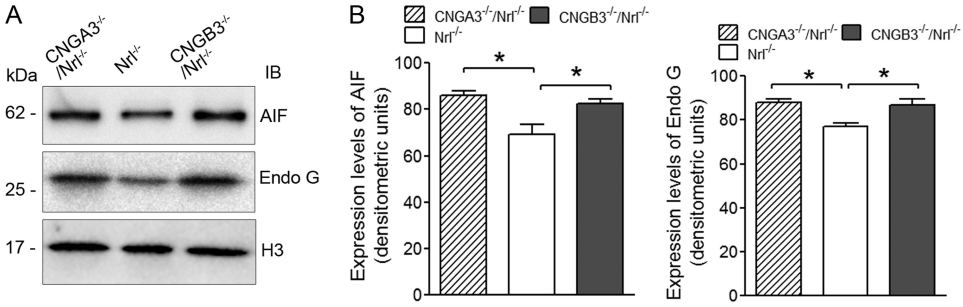

FIGURE 7. **Expression of mitochondrial apoptotic proteins in *CNGA3*$^{-/-}$/*Nrl*$^{-/-}$ and *CNGB3*$^{-/-}$/*Nrl*$^{-/-}$ retinas.** The expression levels of the mitochondrial proteins AIF and Endo G were examined in *CNGA3*$^{-/-}$/*Nrl*$^{-/-}$, *CNGB3*$^{-/-}$/*Nrl*$^{-/-}$, and *Nrl*$^{-/-}$ mice at P30. *A*, shown are representative images of the Western blot detections of AIF and Endo G. Retinal nuclear fractions were used for this examination, and H3 was used as a loading control. *B*, densitometric analysis of the relative levels of AIF and Endo G in the *CNGA3*$^{-/-}$/*Nrl*$^{-/-}$, *CNGB3*$^{-/-}$/*Nrl*$^{-/-}$, and *Nrl*$^{-/-}$ retina. Data are represented as means ± S.E. of measurements from three independent experiments using retinas from four to five mice. Unpaired Student's *t* test was used for determination of the significance (*, $p < 0.05$). *IB*, immunoblot.

pared with the *Nrl*$^{-/-}$ controls. Densitometric analysis shows that the levels of AIF and Endo G were elevated by ~25 and 16%, respectively, in *CNGA3*$^{-/-}$/*Nrl*$^{-/-}$ mice and elevated by ~19 and 14%, respectively, in *CNGB3*$^{-/-}$/*Nrl*$^{-/-}$ mice, compared with the age-matched *Nrl*$^{-/-}$ controls (Fig. 7*B*). This observation suggests a potential mitochondrial insult in CNG channel-deficient retina.

Activation of caspase-3 by caspase-9 following the leakage of cytochrome *c* from mitochondria and the formation of apoptosome is a well characterized cellular event in apoptotic cell death. We therefore examined the levels of cytochrome *c*, caspase-9, and caspase-3 in *CNGA3*$^{-/-}$/*Nrl*$^{-/-}$ and *CNGB3*$^{-/-}$/*Nrl*$^{-/-}$ retinas and found that the levels of these proteins were not altered, and no cleaved forms of caspase-3 or caspase-9 were detected in the channel-deficient retina (data not shown). This observation does not favor a role of the caspase-3-mediated classical pathway in cone death.

DISCUSSION

This work investigated the mechanism(s) of cone degeneration in CNG channel deficiency using *CNGA3*$^{-/-}$/*Nrl*$^{-/-}$ and *CNGB3*$^{-/-}$/*Nrl*$^{-/-}$ mice. Nrl is a basic motif leucine zipper (bZIP) transcription factor essential for the normal development of rods and the *Nrl*$^{-/-}$ mouse line is a cone-dominant mouse model. *Nrl*$^{-/-}$ mice have no rods but have increased numbers of S-cones, functionally manifested as a loss of rod function coupled with super-normal cone function (36). Retinas of *Nrl*$^{-/-}$ mice have cone-like nuclear morphology, short and disorganized OS, and a rosette-like structure (36), and *Nrl*$^{-/-}$ cones undergo a slow degeneration that can result in decreased ERG recordings (~30% reduction) by 2–3 months of age (37, 38). Nevertheless, as a unique mammalian cone-dominant model, the *Nrl*$^{-/-}$ mouse line has been widely used for the study of cone biology and disease (26, 38, 39). We have previously shown that the retinas of *Nrl*$^{-/-}$ mice express an abundant amount of cone CNG channel and lack the expression of the rod channel (25). In this study, we show that the double knock-out mice showed a retinal phenotype similar to that in their respective single knock-out mice, *i.e.* impaired cone function and cone degeneration. Hence, the *CNGA3*$^{-/-}$/*Nrl*$^{-/-}$ and *CNGB3*$^{-/-}$/*Nrl*$^{-/-}$ mouse lines can serve as unique models to explore the mechanism(s) of cone degeneration, particularly to study the biochemical alterations occurring in these mice at young ages.

ER stress has been implicated in a variety of retinal degeneration including those caused by rhodopsin mutations (22, 40) and by deficiency of PDE6 (20, 23). The present work shows ER stress and its associated cell death process in CNG channel-deficient retinas. Although the exact mechanism(s) of ER stress is not known, an altered calcium homeostasis may in part be responsible. As a cellular Ca^{2+} storage organelle, the ER is sensitive to the cellular Ca^{2+} levels. In *rd* mice, lack of the functional PDE6 enzyme causes failure of cGMP degradation, constant opening of the channel and subsequent cellular Ca^{2+} overload, which leads to ER stress (20, 23). In contrast, lack of functional CNG channels might affect the calcium homeostasis differently from that caused by PDE6 deficiency. CNG channel is the only source for Ca^{2+} influx in the OS (1), and lack of the functional CNG channel abolishes the inward Ca^{2+} currents and might potentially lower the cellular Ca^{2+} level. The presumption of a lowered cellular Ca^{2+} level is supported by the observation of cGMP accumulation in CNG channel-deficient retinas (41). Retinal cGMP production is controlled by the enzyme guanylate cyclase-activating protein, which is tightly regulated by the cellular Ca^{2+} level (42). A lowered cellular Ca^{2+} level enhances the activity of guanylate cyclase-activating protein, which in turn stimulates retinal guanylate cyclase to produce cGMP. A low cellular Ca^{2+} level in CNG channel-deficient retina also is supported by the increased levels of phospho-IP_3R and Bcl-2 (which has been shown to modulate Ca^{2+} release from ER storage (43)) (see Fig. 5). It is likely that the lowered cellular Ca^{2+} level evokes Ca^{2+} release from ER storage (via IP_3R). Thus, ER stress in photoreceptors can be evoked by both cellular Ca^{2+} overload (in *rd* mice) (23) and cellular Ca^{2+} insufficiency (in CNG channel deficiency). Of note, our results show that the increases in the ER stress marker proteins (Grp78/Bip, phospho-elF2α, and phospho-IP_3R) were more prominent in *CNGA3*$^{-/-}$/*Nrl*$^{-/-}$ retinas compared with that in *CNGB3*$^{-/-}$/*Nrl*$^{-/-}$ retinas, which may suggest a more severe ER stress in *CNGA3*$^{-/-}$/*Nrl*$^{-/-}$ retina. This observation is consistent with the consequences caused by deficiency of each subunit. Deficiency of CNGA3 causes a complete loss of cone phototransduction, whereas lack of CNGB3 leads to

reduced cone function. Thus, CNGA3 deficiency might cause a much lower cellular Ca^{2+} level compared with that in CNGB3 deficiency. Indeed, we observed a much higher level of retinal cGMP in *CNGA3*$^{-/-}$/*Nrl*$^{-/-}$ mice compared with that in *CNGB3*$^{-/-}$/*Nrl*$^{-/-}$ mice (see supplemental Fig. 1). In a separate experiment, we measured expression of CNGA3 in *CNGB3*$^{-/-}$/*Nrl*$^{-/-}$ retinas by Western blotting. Similar to that in *CNGB3*$^{-/-}$ mice (16), CNGA3 was detected but at a significantly reduced level in *CNGB3*$^{-/-}$/*Nrl*$^{-/-}$ retina (see supplemental Fig. 2). Hence, the remaining light response (mediated by CNGA3 homomeric channels) likely helps maintain the cellular Ca^{2+} levels in *CNGB3*$^{-/-}$/*Nrl*$^{-/-}$ cones.

The ER stress in CNG channel-deficient retinas might also be related with opsin mislocalization and ER accumulation. Accumulation of proteins or misfolded proteins in the ER is known to cause UPR and ER stress. ER stress has been documented in rhodopsin mutation both *in vitro* and *in vivo* (21, 22, 40, 44). *CNGA3*$^{-/-}$ (13) and *CNGB3*$^{-/-}$ (15) mice display opsin mislocalization, and we have shown in this study the co-localization of opsin with Grp78/Bip in the inner segment of *CNGA3*$^{-/-}$ and *CNGB3*$^{-/-}$ retina, supporting an ER accumulation of cone opsin. How deficiency of CNG channel leads to ER accumulation of opsin is still not clear. The phenotype might not be caused directly by the channel deficiency but is more likely a consequence of the loss of (CNGA3 deficiency) or impaired (CNGB3 deficiency) phototransduction. It is worth mentioning that though lack of cone function in the absence of CNG channel (such as in *CNGA3*$^{-/-}$ mice) causes opsin mislocalization, subunit mislocalization arising from disease-linked missense mutations in CNGA3 has been reported extensively in heterologous expression system. Enhanced cytosolic aggregation and activation of ER stress were observed in many CNGA3 mutants, including those with mutations located in the subunit transmembrane S1 and S4 domains (45, 46) and at the carboxyl terminals (47–49). Thus, the UPR and ER stress in CNGA3 missense (and loss of function) mutations could be caused not only by opsin mislocalization (due to lack of normal channel function/phototransduction) but also by mislocalization of mutant CNGA3 subunits, and the ER stress might be more severe than the situation of lack of CNGA3.

Persistent ER stress is known to trigger apoptotic cell death (32). The elevated expression and processing of CHOP, calpains, and caspase-12 suggest an ER stress-associated cell death mechanism in CNG channel deficiency. Based on our findings, we postulate that cone death is likely mediated by the following pathways (Fig. 8).

Grp78/Bip-eIF2a-CHOP Pathway—CHOP is known to be induced by ER stress (28) and by alterations of Ca^{2+} flux across the ER membrane (50). We observed increased levels of CHOP and elevations of Grp78/Bip and phospho-eIF2α in CNG channel-deficient retinas, implying an ER stress-activated, CHOP-mediated cell death. Indeed, CHOP activation has been shown in P23H rhodopsin transgenic rats (51), *Lrat*$^{-/-}$ mice (52), and in rat models of experimental retinal detachment (19).

Calpain-caspase-12 and Calpain-caspase-7-caspase-12 Pathways—It has been shown that calpains are activated in ER stress and mediate processing of caspase-12 (31, 32), and the processed forms translocate to the nucleus to induce apoptosis

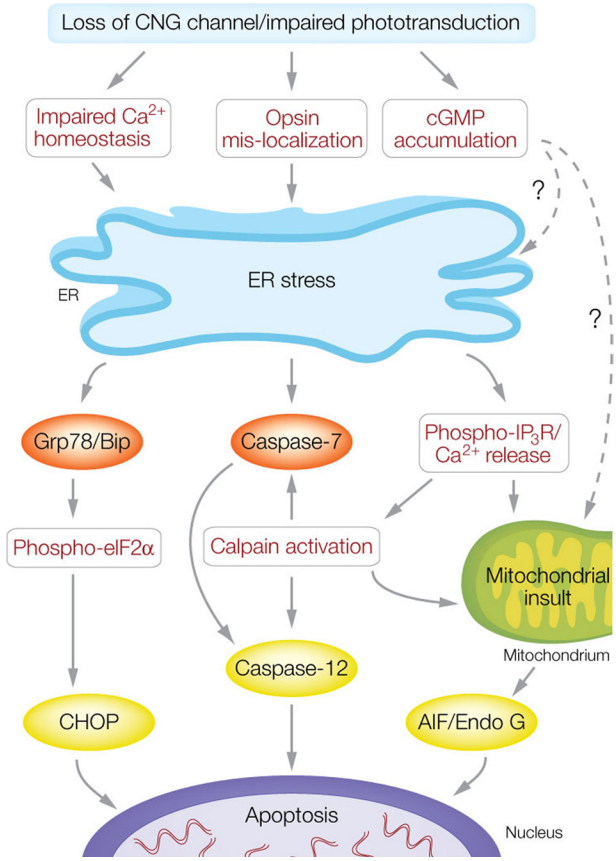

FIGURE 8. **ER stress-associated cone death in CNG channel deficiency.** Loss of functional CNG channel leads to impaired phototransduction. Impaired cone function interferes with the calcium homeostasis and opsin OS localization, which elicits ER stress. The substantial and constant ER stress ultimately triggers apoptotic death through activation of CHOP, caspase-12, and AIF/Endo G pathways. CHOP is induced by the Grp78/Bip and phosho-eIF2α pathway; activation of caspase-12 occurs through caspase-7 and calpains; and activation of mitochondrial AIF and Endo G is mediated by activation of calpains. The altered calcium homeostasis stimulates Ca^{2+} release from ER storage (via IP_3R), which activates calpains. The accumulation of cGMP might be a potential factor to induce ER stress and mitochondrial insult through unknown mechanism(s).

(53). We found elevated expression of calpains, enhanced processing of caspase-12, and nuclear localization of its processed forms in the *CNGA3*$^{-/-}$/*Nrl*$^{-/-}$ and *CNGB3*$^{-/-}$/*Nrl*$^{-/-}$ retinas. These observations suggest that caspase-12 might act as an executioner caspase, and the calpain-caspase-12 pathway might be potentially activated in CNG channel-deficient cones. Indeed, activation of calpains and caspase-12 has been linked to a variety of neurodegenerative conditions, including photoreceptor death in *rd* mice (20, 29, 54). Calpains have also been shown to cleave caspase-7 (34). This processing generates highly active and distinct fragments of caspase-7, which cleave caspase-12 (34). We examined the expression and processing of caspase-7 and found that the full-length protein was detected universally, whereas the processed forms were detected only in the *CNGA3*$^{-/-}$/*Nrl*$^{-/-}$ and *CNGB3*$^{-/-}$/*Nrl*$^{-/-}$ retinas. Hence, activation of caspase-7 might also be involved in cone death. Unlike caspase-12, the processed forms of caspase-7 were not detected in the nuclear fractions, suggesting that caspase-7 acts primarily as an activating caspase. It is likely that caspase-12 is processed by both calpains and caspase-7 in CNG channel-deficient cones.

Calpain-AIF Pathway—ER stress and activation of calpains have been shown to insult mitochondria, manifested as an increased permeability of the mitochondrial membrane and release of AIF. The released AIF can further translocate into the nucleus to induce DNA fragmentation and chromatin condensation (55). The activation of calpains and AIF have been shown in variety of retinal degeneration animal models, including *rd* mice (20, 54), RCS rat (56), and *Uchl3*$^{-/-}$ mice (57). We found an enhanced AIF level in the nuclear fractions of CNG channel-deficient retinas. This observation, along with the elevated calpains, suggests an activated calpain-AIF pathway, a process in which both the ER and mitochondria functions are engaged. Although we observed an increase of AIF in the *CNGA3*$^{-/-}$/*Nrl*$^{-/-}$ and *CNGB3*$^{-/-}$/*Nrl*$^{-/-}$ retina, the mitochondria-mediated, caspase-dependent pathways do not seem to play a major role in cone degeneration. This was supported by the findings that expression levels of cytochrome *c*, procaspase-9, and procaspase-3 were not altered, and no cleaved forms of caspase-3 or caspase-9 were detected in CNG channel-deficient retina. Indeed caspase-3, the executioner caspase in the classical mitochondrion-mediated pathway, appears to play a different role in varying types of photoreceptor degeneration. Activation of caspase-3 was detected in transgenic rats with rhodopsin mutations (58), and use of a caspase-3 inhibitor reduced the apoptotic cell death in *tubby* mice (59); however, photoreceptor death in *rd1* mice was shown to be caspase-3-independent (60), and lack of caspase-3 activation was also reported in animal models of induced retinal degeneration (light damage and retinal detachment) (19). Thus, though apoptotic cell death has been shown as a common cause of many types of photoreceptor degeneration (17), multiple and distinct pathways are likely engaged (61), and the mechanisms might vary between different pathological disorders.

It is important to mention that UPR and ER stress is an evolutionarily conserved cellular program that is characterized by down-regulation of *de novo* protein synthesis, up-regulation of ER chaperones and folding enzymes, and enhanced ER-associated degradation. Thus, UPR and ER stress are protective under certain circumstances. The consequences of ER stress include initiation of both cell death and cell protection from further death, and the balance of the two forces determines the final outcome (62). Recently, delivery of the Grp78/Bip transgene has been shown to reduce CHOP levels and apoptosis and restore visual function in P23H rhodopsin transgenic rats (51). Bcl2 family proteins have been shown to suppress the ER stress-induced caspase activation and cell death (63). Indeed, Bcl and Bcl-x were found to be up-regulated in CNG channel-deficient retina, and they may act as anti-apoptotic factors over the course of cone degeneration.

In summary, cone photoreceptors with CNG channel deficiency undergo ER stress as characterized by elevated levels of Grp78/Bip, phospho-eIF2α, and phospho-IP$_3$R. Accumulation of CHOP in the nucleus, elevated expression of calpains, and processing of caspase-12 and caspase-7 imply an ER stress-associated apoptosis. In addition, the nuclear translocation of AIF and Endo G suggests a mitochondrial insult in the ER stress-associated cell death process.

Acknowledgments—We thank Dr. Anand Swaroop for providing the Nrl$^{-/-}$ *mouse line. We thank Drs. Cheryl Craft and Muna Naash for providing antibodies for M-opsin, S-opsin, and cone arrestin. We thank Jori Avery for technical assistance.*

REFERENCES

1. Kaupp, U. B., and Seifert, R. (2002) Cyclic nucleotide-gated ion channels. *Physiol. Rev.* **82,** 769–824
2. Gerstner, A., Zong, X., Hofmann, F., and Biel, M. (2000) Molecular cloning and functional characterization of a new modulatory cyclic nucleotide-gated channel subunit from mouse retina. *J. Neurosci.* **20,** 1324–1332
3. Zheng, J., Trudeau, M. C., and Zagotta, W. N. (2002) Rod cyclic nucleotide-gated channels have a stoichiometry of three CNGA1 subunits and one CNGB1 subunit. *Neuron* **36,** 891–896
4. Weitz, D., Ficek, N., Kremmer, E., Bauer, P. J., and Kaupp, U. B. (2002) Subunit stoichiometry of the CNG channel of rod photoreceptors. *Neuron* **36,** 881–889
5. Zhong, H., Molday, L. L., Molday, R. S., and Yau, K. W. (2002) The heteromeric cyclic nucleotide-gated channel adopts a 3A:1B stoichiometry. *Nature* **420,** 193–198
6. Shuart, N. G., Haitin, Y., Camp, S. S., Black, K. D., and Zagotta, W. N. (2011) Molecular mechanism for 3:1 subunit stoichiometry of rod cyclic nucleotide-gated ion channels. *Nat. Commun.* **2,** 457
7. Kohl, S., Baumann, B., Broghammer, M., Jägle, H., Sieving, P., Kellner, U., Spegal, R., Anastasi, M., Zrenner, E., Sharpe, L. T., and Wissinger, B. (2000) Mutations in the CNGB3 gene encoding the beta-subunit of the cone photoreceptor cGMP-gated channel are responsible for achromatopsia (ACHM3) linked to chromosome 8q21. *Hum. Mol. Genet.* **9,** 2107–2116
8. Nishiguchi, K. M., Sandberg, M. A., Gorji, N., Berson, E. L., and Dryja, T. P. (2005) Cone cGMP-gated channel mutations and clinical findings in patients with achromatopsia, macular degeneration, and other hereditary cone diseases. *Hum. Mutat.* **25,** 248–258
9. Wissinger, B., Gamer, D., Jägle, H., Giorda, R., Marx, T., Mayer, S., Tippmann, S., Broghammer, M., Jurklies, B., Rosenberg, T., Jacobson, S. G., Sener, E. C., Tatlipinar, S., Hoyng, C. B., Castellan, C., Bitoun, P., Andreasson, S., Rudolph, G., Kellner, U., Lorenz, B., Wolff, G., Verellen-Dumoulin, C., Schwartz, M., Cremers, F. P., Apfelstedt-Sylla, E., Zrenner, E., Salati, R., Sharpe, L. T., and Kohl, S. (2001) CNGA3 mutations in hereditary cone photoreceptor disorders. *Am. J. Hum. Genet.* **69,** 722–737
10. Varsányi, B., Somfai, G. M., Lesch, B., Vámos, R., and Farkas, A. (2007) Optical coherence tomography of the macula in congenital achromatopsia. *Invest. Ophthalmol. Vis. Sci.* **48,** 2249–2253
11. Thiadens, A. A., Somervuo, V., van den Born, L. I., Roosing, S., van Schooneveld, M. J., Kuijpers, R. W., van Moll-Ramirez, N., Cremers, F. P., Hoyng, C. B., and Klaver, C. (2010) Progressive loss of cones in achromatopsia: An imaging study using spectral domain optical coherence tomography. *Invest. Ophthalmol. Vis. Sci.* **51,** 5952–5957
12. Genead, M. A., Fishman, G. A., Rha, J., Dubis, A. M., Bonci, D. M., Dubra, A., Stone, E. M., Neitz, M., and Carroll, J. (2011) Photoreceptor structure and function in patients with congenital achromatopsia. *Invest. Ophthalmol. Vis. Sci.* **52,** 7298–7308
13. Michalakis, S., Geiger, H., Haverkamp, S., Hofmann, F., Gerstner, A., and Biel, M. (2005) Impaired opsin targeting and cone photoreceptor migration in the retina of mice lacking the cyclic nucleotide-gated channel CNGA3. *Invest. Ophthalmol. Vis. Sci.* **46,** 1516–1524
14. Biel, M., Seeliger, M., Pfeifer, A., Kohler, K., Gerstner, A., Ludwig, A., Jaissle, G., Fauser, S., Zrenner, E., and Hofmann, F. (1999) Selective loss of cone function in mice lacking the cyclic nucleotide-gated channel CNG3. *Proc. Natl. Acad. Sci. U.S.A.* **96,** 7553–7557
15. Xu, J., Morris, L., Fliesler, S. J., Sherry, D. M., and Ding, X. Q. (2011). *Invest. Ophthalmol. Vis. Sci.* **52,** 3557–3566
16. Ding, X. Q., Harry, C. S., Umino, Y., Matveev, A. V., Fliesler, S. J., and Barlow, R. B. (2009) Impaired cone function and cone degeneration resulting from CNGB3 deficiency: Down-regulation of CNGA3 biosynthesis as a potential mechanism. *Hum. Mol. Genet.* **18,** 4770–4780

17. Remé, C. E., Grimm, C., Hafezi, F., Marti, A., and Wenzel, A. (1998) Apoptotic cell death in retinal degenerations. *Prog. Retin. Eye Res.* **17,** 443–464
18. Wenzel, A., Grimm, C., Samardzija, M., and Remé, C. E. (2005) Molecular mechanisms of light-induced photoreceptor apoptosis and neuroprotection for retinal degeneration. *Prog. Retin. Eye Res.* **24,** 275–306
19. Liu, H., Qian, J., Wang, F., Sun, X., Xu, X., Xu, W., and Zhang, X. (2010) Expression of two endoplasmic reticulum stress markers, GRP78 and GADD153, in rat retinal detachment model and its implication. *Eye* **24,** 137–144
20. Sanges, D., Comitato, A., Tammaro, R., and Marigo, V. (2006) Apoptosis in retinal degeneration involves cross-talk between apoptosis-inducing factor (AIF) and caspase-12 and is blocked by calpain inhibitors. *Proc. Natl. Acad. Sci. U.S.A.* **103,** 17366–17371
21. Tam, B. M., and Moritz, O. L. (2006) Characterization of rhodopsin P23H-induced retinal degeneration in a *Xenopus laevis* model of retinitis pigmentosa. *Invest. Ophthalmol. Vis. Sci.* **47,** 3234–3241
22. Tam, B. M., Xie, G., Oprian, D. D., and Moritz, O. L. (2006) Mislocalized rhodopsin does not require activation to cause retinal degeneration and neurite outgrowth in *Xenopus laevis*. *J. Neurosci.* **26,** 203–209
23. Yang, L. P., Wu, L. M., Guo, X. J., and Tso, M. O. (2007) Activation of endoplasmic reticulum stress in degenerating photoreceptors of the rd1 mouse. *Invest. Ophthalmol. Vis. Sci.* **48,** 5191–5198
24. Peachey, N. S., Goto, Y., al-Ubaidi, M. R., and Naash, M. I. (1993) Properties of the mouse cone-mediated electroretinogram during light adaptation. *Neurosci. Lett.* **162,** 9–11
25. Matveev, A. V., Quiambao, A. B., Browning Fitzgerald, J., and Ding, X. Q. (2008) Native cone photoreceptor cyclic nucleotide-gated channel is a heterotetrameric complex comprising both CNGA3 and CNGB3: A study using the cone-dominant retina of $Nrl^{-/-}$ mice. *J. Neurochem.* **106,** 2042–2055
26. Kunchithapautham, K., Coughlin, B., Crouch, R. K., and Rohrer, B. (2009) Cone outer segment morphology and cone function in the $Rpe65^{-/-}$ $Nrl^{-/-}$ mouse retina are amenable to retinoid replacement. *Invest. Ophthalmol. Vis. Sci.* **50,** 4858–4864
27. Szegezdi, E., Logue, S. E., Gorman, A. M., and Samali, A. (2006) Mediators of endoplasmic reticulum stress-induced apoptosis. *EMBO Rep.* **7,** 880–885
28. Li, J., Lee, B., and Lee, A. S. (2006) Endoplasmic reticulum stress-induced apoptosis: multiple pathways and activation of p53-up-regulated modulator of apoptosis (PUMA) and NOXA by p53. *J. Biol. Chem.* **281,** 7260–7270
29. Paquet-Durand, F., Azadi, S., Hauck, S. M., Ueffing, M., van Veen, T., and Ekström, P. (2006) Calpain is activated in degenerating photoreceptors in the rd1 mouse. *J. Neurochem.* **96,** 802–814
30. Wang, X., Olberding, K. E., White, C., and Li, C. (2011) Bcl-2 proteins regulate ER membrane permeability to luminal proteins during ER stress-induced apoptosis. *Cell Death Differ.* **18,** 38–47
31. Nakagawa, T., and Yuan, J. (2000) Cross-talk between two cysteine protease families. Activation of caspase-12 by calpain in apoptosis. *J. Cell Biol.* **150,** 887–894
32. Nakagawa, T., Zhu, H., Morishima, N., Li, E., Xu, J., Yankner, B. A., and Yuan, J. (2000) Caspase-12 mediates endoplasmic reticulum-specific apoptosis and cytotoxicity by amyloid-β. *Nature* **403,** 98–103
33. Saini, R. V., Wilson, C., Finn, M. W., Wang, T., Krensky, A. M., and Clayberger, C. (2011) Granulysin delivered by cytotoxic cells damages endoplasmic reticulum and activates caspase-7 in target cells. *J. Immunol.* **186,** 3497–3504
34. Rao, R. V., Hermel, E., Castro-Obregon, S., del Rio, G., Ellerby, L. M., Ellerby, H. M., and Bredesen, D. E. (2001) Coupling endoplasmic reticulum stress to the cell death program. Mechanism of caspase activation. *J. Biol. Chem.* **276,** 33869–33874
35. Li, L. Y., Luo, X., and Wang, X. (2001) Endonuclease G is an apoptotic DNase when released from mitochondria. *Nature* **412,** 95–99
36. Mears, A. J., Kondo, M., Swain, P. K., Takada, Y., Bush, R. A., Saunders, T. L., Sieving, P. A., and Swaroop, A. (2001) Nrl is required for rod photoreceptor development. *Nat. Genet.* **29,** 447–452
37. Daniele, L. L., Lillo, C., Lyubarsky, A. L., Nikonov, S. S., Philp, N., Mears, A. J., Swaroop, A., Williams, D. S., and Pugh, E. N., Jr. (2005) Cone-like morphological, molecular, and electrophysiological features of the photoreceptors of the Nrl knock-out mouse. *Invest. Ophthalmol. Vis. Sci.* **46,** 2156–2167
38. Farjo, R., Skaggs, J. S., Nagel, B. A., Quiambao, A. B., Nash, Z. A., Fliesler, S. J., and Naash, M. I. (2006) Retention of function without normal disc morphogenesis occurs in cone but not rod photoreceptors. *J. Cell Biol.* **173,** 59–68
39. Zhu, X., Brown, B., Li, A., Mears, A. J., Swaroop, A., and Craft, C. M. (2003) GRK1-dependent phosphorylation of S and M opsins and their binding to cone arrestin during cone phototransduction in the mouse retina. *J. Neurosci.* **23,** 6152–6160
40. Griciuc, A., Aron, L., Roux, M. J., Klein, R., Giangrande, A., and Ueffing, M. (2010) Inactivation of cvp/ter94 suppresses retinal pathology caused by misfolded rhodopsin in *Drosophila*. *PLoS Genet.* **6,** pii: e1001075
41. Michalakis, S., Mühlfriedel, R., Tanimoto, N., Krishnamoorthy, V., Koch, S., Fischer, M. D., Becirovic, E., Bai, L., Huber, G., Beck, S. C., Fahl, E., Büning, H., Paquet-Durand, F., Zong, X., Gollisch, T., Biel, M., and Seeliger, M. W. (2010) Restoration of cone vision in the CNGA3-/- mouse model of congenital complete lack of cone photoreceptor function. *Mol. Ther.* **18,** 2057–2063
42. Olshevskaya, E. V., Ermilov, A. N., and Dizhoor, A. M. (2002) Factors that affect regulation of cGMP synthesis in vertebrate photoreceptors and their genetic link to human retinal degeneration. *Mol. Cell Biochem.* **230,** 139–147
43. Palmer, A. E., Jin, C., Reed, J. C., and Tsien, R. Y. (2004) Bcl-2-mediated alterations in endoplasmic reticulum Ca^{2+} analyzed with an improved genetically encoded fluorescent sensor. *Proc. Natl. Acad. Sci. U.S.A.* **101,** 17404–17409
44. Griciuc, A., Aron, L., Piccoli, G., and Ueffing, M. (2010) Clearance of Rhodopsin(P23H) aggregates requires the ERAD effector VCP. *Biochim. Biophys. Acta* **1803,** 424–434
45. Patel, K. A., Bartoli, K. M., Fandino, R. A., Ngatchou, A. N., Woch, G., Carey, J., and Tanaka, J. C. (2005) Transmembrane S1 mutations in CNGA3 from achromatopsia 2 patients cause loss of function and impaired cellular trafficking of the cone CNG channel. *Invest. Ophthalmol. Vis. Sci.* **46,** 2282–2290
46. Faillace, M. P., Bernabeu, R. O., and Korenbrot, J. I. (2004) Cellular processing of cone photoreceptor cyclic GMP-gated ion channels: A role for the S4 structural motif. *J. Biol. Chem.* **279,** 22643–22653
47. Reuter, P., Koeppen, K., Ladewig, T., Kohl, S., Baumann, B., and Wissinger, B. (2008) Mutations in CNGA3 impair trafficking or function of cone cyclic nucleotide-gated channels, resulting in achromatopsia. *Hum. Mutat.* **29,** 1228–1236
48. Matveev, A. V., Fitzgerald, J. B., Xu, J., Malykhina, A. P., Rodgers, K. K., and Ding, X. Q. (2010) The disease-causing mutations in the carboxyl terminus of the cone cyclic nucleotide-gated channel CNGA3 subunit alter the local secondary structure and interfere with the channel active conformational change. *Biochemistry* **49,** 1628–1639
49. Duricka, D. L., Brown, R. L., and Varnum, M. D. (2012) Defective trafficking of cone photoreceptor CNG channels induces the unfolded protein response and ER stress-associated cell death. *Biochem. J.* **441,** 685–696
50. Wang, X. Z., Lawson, B., Brewer, J. W., Zinszner, H., Sanjay, A., Mi, L. J., Boorstein, R., Kreibich, G., Hendershot, L. M., and Ron, D. (1996) Signals from the stressed endoplasmic reticulum induce C/EBP-homologous protein (CHOP/GADD153). *Mol. Cell. Biol.* **16,** 4273–4280
51. Gorbatyuk, M. S., Knox, T., LaVail, M. M., Gorbatyuk, O. S., Noorwez, S. M., Hauswirth, W. W., Lin, J. H., Muzyczka, N., and Lewin, A. S. (2010) Restoration of visual function in P23H rhodopsin transgenic rats by gene delivery of BiP/Grp78. *Proc. Natl. Acad. Sci. U.S.A.* **107,** 5961–5966
52. Zhang, T., Zhang, N., Baehr, W., and Fu, Y. (2011) Cone opsin determines the time course of cone photoreceptor degeneration in Leber congenital amaurosis. *Proc. Natl. Acad. Sci. U.S.A.* **108,** 8879–8884
53. Fujita, E., Kouroku, Y., Jimbo, A., Isoai, A., Maruyama, K., and Momoi, T. (2002) Caspase-12 processing and fragment translocation into nuclei of tunicamycin-treated cells. *Cell Death Differ.* **9,** 1108–1114
54. Sanges, D., and Marigo, V. (2006) Cross-talk between two apoptotic pathways activated by endoplasmic reticulum stress: Differential contribution

of caspase-12 and AIF. *Apoptosis* **11,** 1629–1641
55. Polster, B. M., Basañez, G., Etxebarria, A., Hardwick, J. M., and Nicholls, D. G. (2005) Calpain I induces cleavage and release of apoptosis-inducing factor from isolated mitochondria. *J. Biol. Chem.* **280,** 6447–6454
56. Mizukoshi, S., Nakazawa, M., Sato, K., Ozaki, T., Metoki, T., and Ishiguro, S. (2010) Activation of mitochondrial calpain and release of apoptosis-inducing factor from mitochondria in RCS rat retinal degeneration. *Exp. Eye Res.* **91,** 353–361
57. Sano, Y., Furuta, A., Setsuie, R., Kikuchi, H., Wang, Y. L., Sakurai, M., Kwon, J., Noda, M., and Wada, K. (2006) Photoreceptor cell apoptosis in the retinal degeneration of Uchl3-deficient mice. *Am. J. Pathol.* **169,** 132–141
58. Liu, C., Li, Y., Peng, M., Laties, A. M., and Wen, R. (1999) Activation of caspase-3 in the retina of transgenic rats with the rhodopsin mutation s334ter during photoreceptor degeneration. *J. Neurosci.* **19,** 4778–4785
59. Bode, C., and Wolfrum, U. (2003) Caspase-3 inhibitor reduces apototic photoreceptor cell death during inherited retinal degeneration in tubby mice. *Mol. Vis.* **9,** 144–150
60. Doonan, F., Donovan, M., and Cotter, T. G. (2003) Caspase-independent photoreceptor apoptosis in mouse models of retinal degeneration. *J. Neurosci.* **23,** 5723–5731
61. Doonan, F., Donovan, M., and Cotter, T. G. (2005) Activation of multiple pathways during photoreceptor apoptosis in the rd mouse. *Invest. Ophthalmol. Vis. Sci.* **46,** 3530–3538
62. Mendes, C. S., Levet, C., Chatelain, G., Dourlen, P., Fouillet, A., Dichtel-Danjoy, M. L., Gambis, A., Ryoo, H. D., Steller, H., and Mollereau, B. (2009) ER stress protects from retinal degeneration. *EMBO J.* **28,** 1296–1307
63. Murakami, Y., Aizu-Yokota, E., Sonoda, Y., Ohta, S., and Kasahara, T. (2007) Suppression of endoplasmic reticulum stress-induced caspase activation and cell death by the overexpression of Bcl-x_L or Bcl-2. *J. Biochem.* **141,** 401–410